Medicinal Chemistry Research (2019) 28:1694–1703
https://doi.org/10.1007/s00044-019-02406-5

MEDICINAL CHEMISTRY RESEARCH

ORIGINAL RESEARCH

New pyranoquinoline derivatives as vascular-disrupting anticancer agents

Florian Schmitt[1] · Rainer Schobert[1] · Bernhard Biersack[1]

Received: 14 March 2019 / Accepted: 17 July 2019 / Published online: 27 July 2019

Abstract

A series of new 4-aryl-pyranoquinoline derivatives with a focus on *meta*-nitro and *meta*-halophenyl derivatives were prepared and investigated for their structure-dependent antiproliferative effects on a panel of six human cancer cell lines. The compounds were highly active with nanomolar IC_{50} values. Some of them even exceeded the activities of known analogs such as LY290181 in vitro while not affecting non-malignant fibroblasts. These most active derivatives led to an increase of reactive oxygen species in cancer cells and to a disruption of their microtubular cytoskeleton by inhibiting tubulin polymerization. They also displayed vascular-disrupting activity *in ovo* as assessed by chorioallantoic membrane assays.

Keywords Pyranoquinoline · Anticancer agents · Tubulin polymerization inhibitors · Vascular-disrupting agents

Introduction

The heterocyclic quinoline framework is a component of many bioactive compounds, such as antimalarials (quinine and its derivatives) and anticancer agents (camptothecin and its derivatives) (Kumar et al. 2009). In particular, quinoline is an attractive scaffold for anticancer drug design and the relevance of quinolines as potential anticancer drugs was recently reviewed (Afzal et al. 2015). Initial studies of highly anticancer active 4-aryl-substituted pyranoquinolines with IC_{50} values in the nanomolar concentration range were carried out by Kemnitzer and coworkers who focussed on the pro-apoptotic properties of these compounds (Kemnitzer et al. 2007). Another work by El-Agrodi and coworkers disclosed IC_{50} values in the single-digit µg/mL concentration range in cancer cells (El-Agrody et al. 2013). More recently, 4-aryl-pyrano-oxoquinolines were investigated and the 3-chlorophenyl and 3-bromophenyl derivatives showed the strongest antiproliferative activities with IC_{50} values of 0.1–1.0 µM (Upadhyay et al. 2018). 4-Aryl-4*H*-naphthopyrans such as LY290181 (Fig. 1) constitute an important class of microtubule destabilizing compounds with high potential as drug candidates due to their simple and low-cost one-pot preparation (Wiernicki et al. 1996; Wood et al. 1997; Schmitt et al. 2018; Schmitt et al. 2019). LY290181 binds to tubulin in a unique way which might be of significance for the design of new anticancer active tubulin binders with reduced cross-resistance to known ligands of the colchicine-binding site (Wood et al. 1997). In addition, LY290181 suppressed diabetes-induced vascular dysfunction and PKC activity by inhibition of uPA promoter activation in diabetic in vivo models (Birch et al. 1996). Further closely related 4-aryl-naphthopyrans exhibited moderate Src kinase inhibition, displayed antirheumatic and antimicrobial activities, or were designed for restenosis and diabetes treatment (Wiernicki et al. 1996; Rafinejad et al. 2012; Birch et al. 1996; Thumar and Patel 2009; Smith et al. 1995). Recently, various chlorinated or brominated 4-aryl-4*H*-pyrano[3,2-*h*]quinoline derivatives were disclosed that were moderately tumor cell growth inhibitory, however, without any results about their modes of action (Fouda 2017). 4-Fluorophenyl derivatives were not available via this method since the applied piperidine base reacts with the 4-fluorophenyl ring and, thus, fluorophenyl derivatives are very rare (El-Agrody and Al-Ghamdi 2011; Dgachi et al. 2017). However, fluoro-substituted drugs displayed distinct anticancer properties (Isanbor and O'Hagan 2006). Because of this and in continuation of our recent reports on

Supplementary information The online version of this article (https://doi.org/10.1007/s00044-019-02406-5) contains supplementary material, which is available to authorized users.

✉ Bernhard Biersack
bernhard.biersack@yahoo.com

[1] Organic Chemistry Laboratory, University of Bayreuth, Universitätsstrasse 30, 95440 Bayreuth, Germany

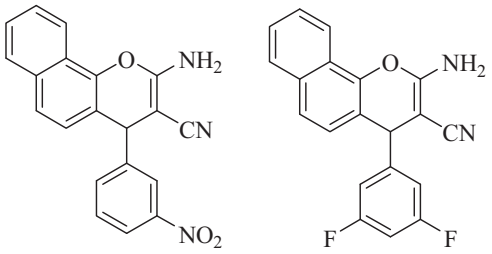

LY290181 **1a**

Fig. 1 Structures of known naphthopyrans LY290181 and **1a**

meta-fluorinated 4-aryl-4*H*-naphthopyrans as anticancer active tubulin-binding compounds with strong in vitro and in vivo anticancer activities (e.g., compound **1a**, Fig. 1) we synthesized and examined analogous new 4-aryl-4*H*-pyrano [3,2-*h*]quinoline derivatives for their potential as anticancer agents in this study (Schmitt et al. 2018; Schmitt et al. 2019).

The disruption of the tumor vascular system in order to deprive the tumor cells of nutrients and oxygen is a promising field of oncological research (Thorpe 2002). The disruption of tumor blood vessels by vascular-disrupting agents (VDAs) is often associated with microtubule destabilization (Pérez-Pérez et al. 2016). Most of the investigated VDAs are derivatives of the natural products colchicine and combretastatin A4 (CA-4), which share the 1,2,3-trimethoxyphenyl motif and target the colchicine-binding site of tubulin. Their relatively simple structure paved the way to the synthesis and biological evaluation of numerous colchicine and combretastatin derivatives (Pérez-Pérez et al. 2016; Lippert 2007; Tron et al. 2006). As mentioned above, both LY290181 and compound **1a** have already been shown to affect the vascularisation. Hence, the effects of the new compounds on tubulin dynamics and tissue vascularisation were studied in this work as well.

Results and discussion

Chemistry

The new 4-aryl-pyranoquinolines of this study were prepared following a one-pot literature procedure (El-Agrody et al. 2013). In detail, malononitrile and the respective aryl aldehyde were reacted to give the corresponding arylidenemalononitrile intermediates under base catalysis. The latter afforded the desired 4-aryl-4*H*-pyranoquinolines upon addition of 8-hydroxyquinoline or 2-methyl-8-hydroxyquinoline, respectively. The products are presented in Scheme 1. They were obtained as colorless, off-white, or amber solids (**3d**) in yields between 30 and 62%. The yields could be correlated with solubility in polar organic solvents

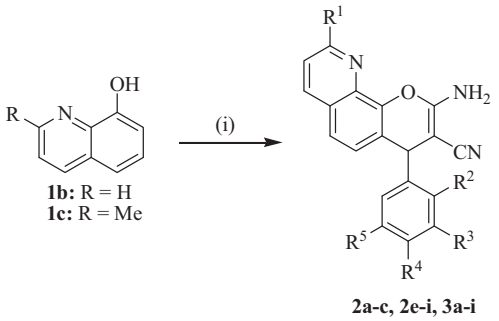

2a-c, 2e-i, 3a-i

Compd. (Yield)	R^1	R^2	R^3	R^4	R^5
2a (33%)	-H	-H	-F	-H	-F
2b	-H	-H	-F	-H	-H
2c	-H	-H	-Cl	-H	-H
2e	-H	-F	-H	-H	-H
2f (38%)	-H	-H	-Br	-H	-H
2g (48%)	-H	-F	-F	-H	-H
2h (57%)	-H	-F	-H	-H	-F
2i (34%)	-H	-H	-F	-OMe	-H
3a (30%)	$-CH_3$	-H	-F	-H	-F
3b (30%)	$-CH_3$	-H	-F	-H	-H
3c	$-CH_3$	-H	-Cl	-H	-H
3d (31%)	$-CH_3$	-H	$-NO_2$	-H	-H
3e (35%)	$-CH_3$	-F	-H	-H	-H
3f (62%)	$-CH_3$	-H	-Br	-H	-H
3g (32%)	$-CH_3$	-F	-F	-H	-H
3h (49%)	$-CH_3$	-F	-H	-H	-F
3i (33%)	$-CH_3$	-H	-F	-OMe	-H

Scheme 1 Reactions and conditions: (i) malononitrile, aryl aldehyde, cat. piperidine, EtOH, r.t., 30 min, then addition of **1b** or **1c**, reflux, 2.5 h; yields in % are given for new compounds

such as ethanol, the better the solubility the poorer the yields. 4-Fluorophenyl derivatives were not obtained via the described method, which is in line with published reports (El-Agrody and Al-Ghamdi 2011).

Antiproliferative activity

MTT assays were carried out in order to determine the antiproliferative activity of the test compounds. **3b** was not soluble enough to obtain reasonable results. The new quinoline derivative **2a** as well as the new methylquinolines **3a**, **3d**, and **3f** revealed excellent activities with IC_{50} concentrations in the two-digit nanomolar range (Table 1). The difluorinated **3a** and the nitrophenyl derivative **3d** were the most active compounds in most of the examined cancer cell lines including multidrug-resistant cells while exhibiting much lower activities against the drug-sensitive non-malignant human dermal fibroblasts from adult skin (HDFa). Compound **2a** showed the highest activity of all test compounds against the MCF-7^{Topo} breast carcinoma cells. In fact, compounds **2a** and **3a** were more active than LY290181 and **1a** against the MCF-7^{Topo} cells, and **3a** was also more active than LY290181 and **1a** against the KB-$V1^{Vbl}$ cells. Both cell lines are multidrug-resistant with

Table 1 Inhibitory concentrations IC_{50}[a] [nM] of test compounds LY290181, **1a**, **2a–c**, **2e–i**, **3a**, and **3c–i** when applied to cells of human 518A2 melanoma, KB-$V1^{Vbl}$ cervix carcinoma, MCF-7^{Topo} breast carcinoma and HT-29, HCT-116 and DLD-1 colon (adeno-) carcinomas, and non-malignant HDFa

	518A2	HT-29	DLD-1	HCT-116	KB-$V1^{Vbl}$	MCF-7^{Topo}	HDFa
LY290181[b]	35.9 ± 0.8	46.9 ± 3.2	33.7 ± 1.5	44.3 ± 4.3	22.6 ± 3.3	11.8 ± 1.4	–
1a[b]	26.4 ± 0.6	176 ± 19	32.3 ± 3.5	47.0 ± 1.9	25.8 ± 4.3	20.1 ± 0.6	–
2a	89 ± 6	84 ± 8	95 ± 4	97 ± 15	63 ± 13	5.8 ± 0.8	–
2b	508 ± 14	–	–	–	–	–	–
2c	304 ± 16	–	–	–	–	–	–
2e	801 ± 60	–	971 ± 186	585 ± 88	583 ± 24	434 ± 36	–
2f	188 ± 27	167 ± 11	121 ± 5	189 ± 9	116 ± 10	130 ± 36	–
2g	335 ± 33	–	–	–	–	–	–
2h	508 ± 35	–	–	–	–	–	–
2i	> 100,000	–	–	–	–	–	–
3a	66 ± 11	74 ± 10	40 ± 5	47 ± 7	14 ± 2	10 ± 1	>100,000
3c	267 ± 27	–	–	–	–	–	–
3d	45 ± 5	86 ± 7	59 ± 10	80 ± 7	20 ± 6	20 ± 5	>100,000
3e	264 ± 10	–	301 ± 36	360 ± 38	290 ± 7	316 ± 44	–
3f	92 ± 6	201 ± 24	87 ± 7	155 ± 6	59 ± 7	59 ± 13	–
3g	188 ± 19	–	–	–	–	–	–
3h	160 ± 14	–	–	–	–	–	–
3i	4702 ± 241	–	–	–	–	–	–

[a]Values are the means ± SD (standard deviation) of four independent experiments. They were derived from concentration–response curves obtained by measuring the percentage of vital cells relative to untreated controls after 72 h using MTT assays

[b]Values taken from Schmitt et al. 2019

overexpressed drug efflux pumps. In addition, **2a**, **3a**, and **3d** were more active than **1a** against HT-29 cells, which are resistant to the known tubulin polymerization inhibitor combretastatin A-4 ($IC_{50} > 1$ µM after 72 h; Mahal et al. 2013). Methylation of the quinoline fragment in compounds **3** led to an improved growth inhibition in most cancer cell lines except for the MCF-7^{Topo} cells, where analog **2a** performed best, possibly because of a higher lipophilicity of compounds **3** when compared with **2**. The known 3-fluorophenyl and 3-chlorophenyl derivatives **2b**, **2c**, and **3c** showed weaker activities against 518A2 melanoma cells when compared with the 3,5-difluorophenyl-derivatives **2a** and **3a**. The 3-bromophenyl derivatives **2f** and **3f** were more active than the 3-chlorophenyl-derivatives but less active than **2a** and **3a**.

The 2,3- and 2,5-difluorophenyl derivatives **2g** and **2h** showed relatively weak activity against 518A2 cells while the 3-fluoro-4-methoxyphenyl compound **2i** was inactive. The analogous methylquinolines **3g**, **3h**, and **3i** were more active than their nor-congeners but they were also distinctly less active than **3a** and **3d**. Thus, these compounds were not tested against the other cancer cell lines.

Interference with the microtubule cytoskeleton

The new compounds **3a** and **3d** were also tested for their potential inhibition of the microtubule assembly which is a typical feature of vascular-disrupting agents. Their effect on the polymerization of tubulin was determined in vitro using purified pig brain tubulin (Fig. 2). 10 µM of the difluorophenyl derivative **3a** inhibited the polymerization of pig brain tubulin more strongly than the same dose of the analogous 3-nitrophenyl derivative **3d**. The activity of both compounds is comparable with the activity of LY290181 (Schmitt et al. 2019). This inhibition of tubulin polymerization is likely to contribute to the antiproliferative effect of compound **3a** and to a lesser extent to that of compound **3d**. The tubulin polymerization inhibition by **3a**

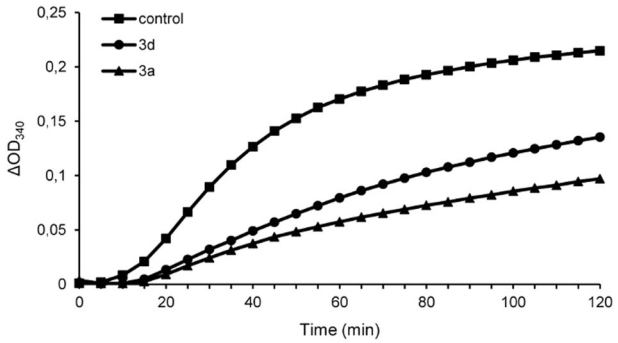

Fig. 2 Effects of compounds **3a** and **3d** (10 µM each) on the polymerization of tubulin as determined by a turbidimetric cell-free tubulin assay. Data are representative of two independent experiments. ΔOD_{340} is the change in the absorption at 340 nm wavelength with OD_{340} set as 0 at 0 min; control: vehicle (DMSO)

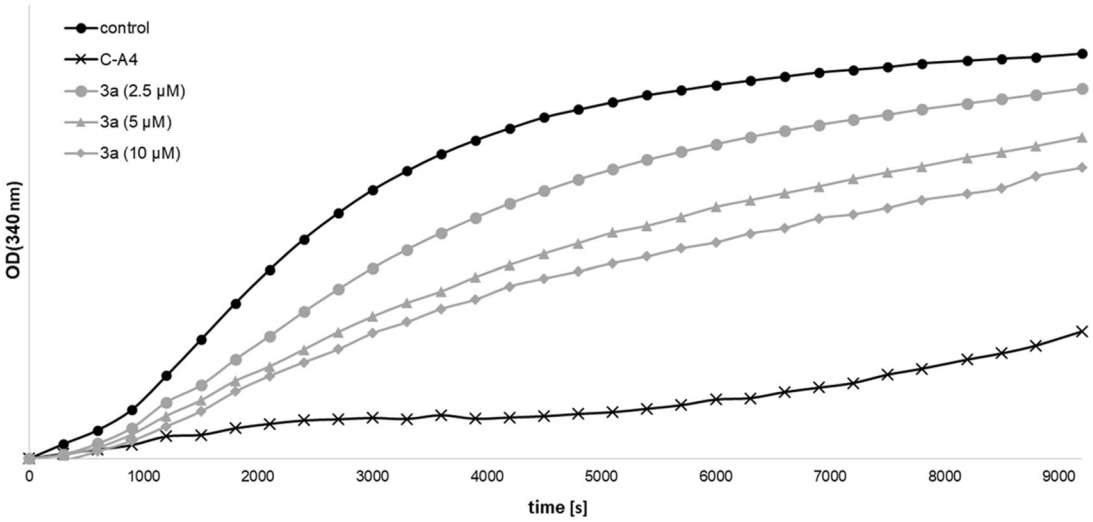

Fig. 3 Effects of various concentrations of compound **3a** and CA-4 (10 µM) on the polymerization of tubulin as determined by a turbidimetric cell-free tubulin assay. Data are representative of two independent experiments. ΔOD_{340} is the change in the absorption at 340 nm wavelength with OD_{340} set as 0 at 0 min; control: vehicle (DMSO)

was dose-dependent and weaker when compared with CA-4 (Fig. 3). The in vitro results were additionally confirmed on a cellular level by immunostaining of alpha-tubulin in 518A2 melanoma cells (Fig. 4). 3-Nitrophenyl derivative **3d** eroded the highly organized microtubule network, but left some intact clusters especially around the nuclei. The blebbed arrangement of the nuclei is a sign of apoptosis induction in these cancer cells treated with **3d**.

ROS formation

The compound-induced ROS generation has been recognized as one of the mechanisms underlying their cytotoxicity since the ROS overproduction induces ER (endoplasmic reticulum) stress and mitochondrial apoptosis (Lau et al. 2008). Previously published naphthopyran derivatives initiated significant ROS productions in cancer cells (Schmitt et al. 2018). Therefore, we investigated the effect of **3a** and **3d** on the intracellular ROS levels in 518A2 melanoma cells using the DCFH-DA (2′,7′-dichlorohydrofluorescein diacetate) assay. After cellular uptake, DCFH-DA is deacetylated by cellular esterases to DCFH (2′,7′-dichlorohydrofluorescein), which is oxidized by ROS to the fluorescent DCF (2′,7′-dichlorofluorescein). Its fluorescence intensity is proportional to the intracellular ROS levels. Both test compounds, **3a** and **3d**, when applied at 10 µM, caused an increase of the cellular ROS levels exceeding 200% compared with the ROS levels of untreated control cells which were set to 100% (Fig. 5). The maximum of ROS production was already reached by the lowest applied concentration of 1 µM. For comparison, the ROS producing agent pyocyanin can cause ROS levels of almost 500% in

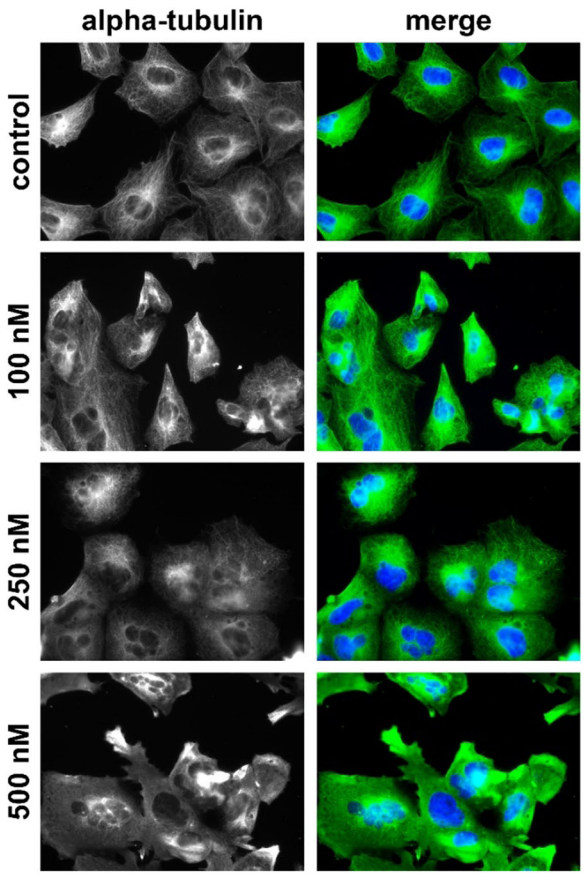

Fig. 4 Effect of compound **3d** (0.1 µM, 0.25 µM, 0.5 µM), and vehicle (DMSO) on the organization of the microtubule cytoskeleton in 518A2 melanoma cells after 24 h incubation. Nuclei were counterstained with DAPI (merge, blue); microtubule (merge, green). Pictures are representative of two independent experiments (×400 magnification)

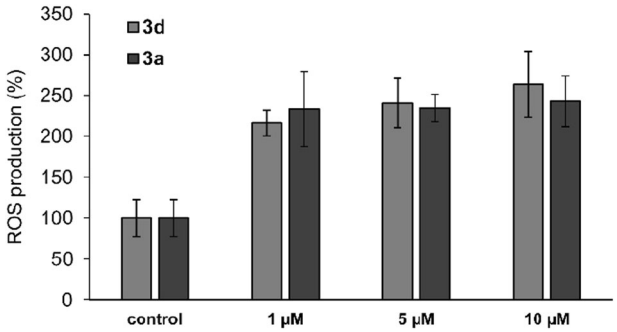

Fig. 5 ROS generation in 518A2 melanoma cells induced by test compounds **3a** and **3d**. After pretreatment of the cells with DCFH-DA (20 µM, 30 min), they were incubated with **3a** or **3d** (0, 1, 5, and 10 µM; 1 h). The green fluorescence of DCF as a measure of the intracellular ROS level was set to 100% for vehicle-treated control cells (0 µM). The ROS generation (%) is depicted as the mean ± SD of five independent experiments. Significant deviations from control data were determined using a *t*-test. A significant increase in ROS-generation was observed for cells treated with **3a** and **3d** (1, 5, and 10 µM; $p < 0.002$) when compared with vehicle-treated control cells

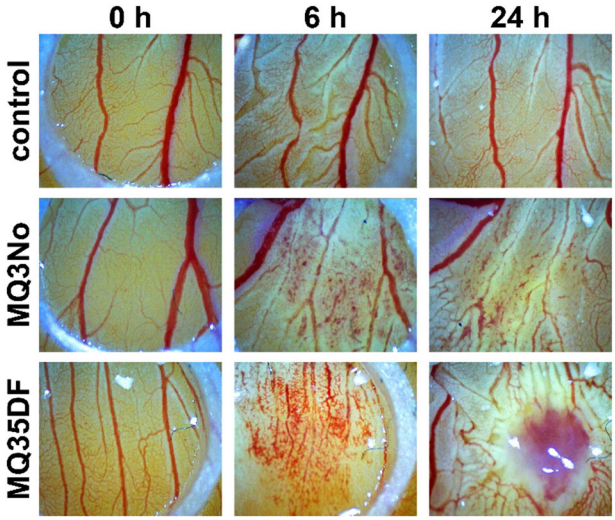

Fig. 6 Effects of complexes **3a** (MQ35DF, 5 nmol) and **3d** (MQ3No, 10 nmol) when applied topically to the vasculature in the chorioallantoic membrane of fertilized chicken eggs at 6 and 24 hpa. Control: respective amount of DMSO. Images are representative of at least three independent experiments (×60 magnification)

518A2 cells after treatment for 1 h at a dose of 100 µM (Gold et al. 2019).

Vascular-disrupting activity

The vascular-disruptive effect of compounds **3a** and **3d** was tested on the chorioallantoic membrane (CAM) of fertilized chicken eggs, which is a suitable and ethically favorable surrogate assay for animal tests. The compounds were applied topically onto the CAM in a small ring of silicon foil next to some main blood vessels. The applied dose of **3a** (5 nmol) was lower than the applied dose of **3d** (10 nmol) since **3a** showed generally higher activities in the MTT assays (see above). Any alterations of the blood vessels were documented 0, 6, and 24 h post application (hpa). The compounds induced the disruption of even big blood vessels and consequently caused hemorrhages already 6 hpa (Fig. 6). However, the compounds differed in their effect on the CAM 24 hpa. While the effect of **3d** focused on the selective destruction of blood vessels of the CAM, the treatment with **3a** led to contraction and irritation of the membrane which is indicative of its general toxicity. The effects by **3a** (5 nmol) were comparable with those observed for **1a** (5 nmol) and LY290181 (5 nmol) after 6 and 24 h (Schmitt et al. 2019).

Conclusion

New vascular-disrupting agents with distinct microtubule cytoskeleton damaging effects were identified. The new compounds **2a**, **3a**, and **3d** exhibited promising tumor cell growth inhibitory activities while not affecting non-malignant fibroblasts. Their superior effect on drug-resistant cancer cell lines is particularly intriguing. The mode of action of compounds **3a** and **3d** may at least in parts be associated with tubulin polymerization interference and ROS formation. In addition, the *in ovo* activity of these compounds concerning vascular disruption in the chorioallantoic membrane of fertilized chicken eggs was confirmed. Thus, these compounds represent suitable drug candidates for the treatment of drug-resistant cancer diseases, as well as of other diseases based on pathological vascularization, such as Osler-Weber-Rendu disease or age-related macular degeneration.

Experimental section

Chemistry

The starting compounds and pure solvents were purchased from the usual sources and were used without further purification. Compounds **1a, 2b, 2c, 2e, 3c**, and LY290181 were prepared after literature procedures and analyzed (NMR, IR, MS) leading to the identification of these compounds as pure compounds (El-Agrody et al. 2013; Dgachi et al. 2017; Schmitt et al. 2019). Melting points: Gallenkamp apparatus (uncorrected). IR: Perkin-Elmer Spectrum One FT-IR spectrophotometer equipped with an ATR sampling unit. NMR: Bruker Avance 300 spectrometer; chemical shifts are given in parts per million (δ) downfield from Me_4Si as internal standard; coupling constants (*J*) are given in Hz; MS: Varian MAT 311A (EI), Varian 1200L

Q3 (ESI); microanalyses: Perkin-Elmer 2400 CHN elemental analyzer. Copies of the ^{1}H NMR, ^{13}C NMR and mass spectra of the new compounds are provided in the supplementary material.

General procedure for the synthesis of 2a–c, 2e–i and 3a–i

A mixture of substituted benzaldehyde (1.0 mmol) and malononitrile (70 mg, 1.0 mmol) was dissolved in EtOH (3 mL) and three drops of piperidine were added with a Pasteur pipette. The reaction mixture was stirred at room temperature for 30 min. 8-Hydroxyquinoline (145 mg, 1.0 mmol) or 2-methyl-8-hydroxyquinoline (159 mg, 1.0 mmol), respectively, was added and the reaction mixture was stirred under reflux for 2.5 h. The formed precipitate was collected, washed with EtOH or EtOH/H_2O mixtures and dried in vacuum.

2-Amino-4-(3,5-difluorophenyl)-4*H*-pyrano[3,2-*h*]quinolone-3-carbonitrile (2a)

Colorless solid; yield 33%; mp 250–252 °C; IR (ATR) υ_{max} 3463, 3331, 3193, 3082, 2196, 1659, 1620, 1596, 1567, 1500, 1467, 1451, 1401, 1387, 1371, 1318, 1308, 1295, 1247, 1224, 1191, 1120, 1106, 1053, 1028, 1005, 990, 957, 864, 832, 816, 806, 784, 744, 692 cm^{-1}; ^{1}H NMR (300 MHz, $CDCl_3$/DMSO-d_6): $\delta = 4.78$ (s, 1H), 5.65 (s, 2H), 6.5–6.7 (m, 3H), 6.99 (d, $J = 8.5$ Hz, 1H), 7.3–7.4 (m, 2H), 8.03 (dd, $J = 8.4$ Hz, 1.6 Hz, 1H), 8.8–8.9 (m, 1H); ^{13}C NMR (75.5 MHz, $CDCl_3$/DMSO-d_6): $\delta = 41.4$, 58.0, 102.3–103.0 (m), 110.6–110.9 (m), 119.4, 120.0, 121.9, 123.8, 126.4, 128.2, 135.8, 137.8, 143.3, 148.1, 148.2, 150.3, 159.8, 161.2–161.4 (m), 164.5–164.7 (m); EIMS *m/z* 335 (97) [M]$^+$, 219 (18), 222 (100), 195 (35), 167 (15), 140 (22); Anal. Calcd. for $C_{19}H_{11}F_2N_3O$: C, 68.06; H, 3.31; N, 12.53. Found: C, 68.11; H, 3.34; N, 12.45.

2-Amino-4-(3-bromophenyl)-4*H*-pyrano[3,2-*h*]quinolone-3-carbonitrile (2f)

Off-white solid; yield 38%; mp 272–273 °C; IR (ATR) υ_{max} 3327, 3184, 2195, 1655, 1627, 1596, 1567, 1499, 1467, 1432, 1402, 1387, 1374, 1316, 1292, 1246, 1184, 1105, 1071, 1049, 1021, 996, 874, 830, 785, 766, 738, 688 cm^{-1}; ^{1}H NMR (300 MHz, $CDCl_3$): $\delta = 4.87$ (s, 1H), 5.15 (s, 2H), 7.09 (d, $J = 8.6$ Hz, 1H), 7.2–7.3 (m, 2H), 7.3–7.4 (m, 2H), 7.4–7.5 (m, 2H), 8.13 (dd, $J = 8.3$ Hz, 1.7 Hz, 1H), 8.9–9.0 (m, 1H); ^{13}C NMR (75.5 MHz, $CDCl_3$): $\delta = 41.5$, 58.4, 119.3, 120.9, 122.2, 123.1, 124.1, 126.8, 127.0, 128.4, 130.5, 130.8, 131.1, 136.2, 138.0, 143.4, 146.4, 150.6, 159.5; EIMS *m/z* 379 (62) [M]$^+$, 377 (64) [M$^+$], 335 (5), 333 (5), 314 (15), 312 (16), 223 (86), 222 (100), 195 (34), 167 (12), 140 (17); Anal. Calcd. for $C_{19}H_{12}BrN_3O$: C, 60.34; H, 3.20; N, 11.11. Found: C, 60.29; H, 3.16; N, 11.14.

2-Amino-4-(2,3-difluorophenyl)-4*H*-pyrano[3,2-*h*]quinolone-3-carbonitrile (2g)

Colorless solid; yield: 48%; mp 278–280 °C; IR (ATR) υ_{max} 3460, 3327, 3188, 3053, 2189, 1652, 1628, 1596, 1567, 1502, 1479, 1470, 1435, 1406, 1388, 1377, 1318, 1291, 1272, 1248, 1188, 1139, 1105, 1057, 1027, 997, 948, 906, 829, 790, 782, 770, 753, 734, 712, 659, 648, 627 cm^{-1}; ^{1}H NMR (300 MHz, DMSO-d_6): $\delta = 5.31$ (s, 1H), 7.0–7.3 (m, 6H), 7.6–7.7 (m, 2H), 8.3–8.4 (m, 1H), 8.9–9.0 (m, 1H); ^{13}C NMR (75.5 MHz, DMSO-d_6): $\delta = 35.6$, 54.0, 116.2–116.5 (m), 119.9–120.0 (m), 122.3, 123.9, 125.1–125.3 (m), 126.4, 128.0, 134.4, 136.0, 137.4, 143.4, 146.1–146.3 (m), 148.1–148.3 (m), 149.4–149.6 (m), 150.4, 151.4–151.5 (m), 160.6; EIMS *m/z* 335 (83) [M$^+$], 291 (13), 222 (100), 195 (19); Anal. Calcd. for $C_{19}H_{11}F_2N_3O$: C, 68.06; H, 3.31; N, 12.53. Found: C, 68.09; H, 3.29; N, 12.48.

2-Amino-4-(2,5-difluorophenyl)-4*H*-pyrano[3,2-*h*]quinolone-3-carbonitrile (2h)

Colorless solid; yield: 57%; mp 272–274 °C; IR (ATR) υ_{max} 3463, 3331, 3188, 3063, 2192, 1653, 1628, 1596, 1567, 1490, 1469, 1405, 1389, 1376, 1318, 1300, 1254, 1213, 1186, 1174, 1131, 1105, 1085, 1049, 1023, 978, 957, 880, 830, 818, 768, 757, 736, 719, 680, 650, 627, 606 cm^{-1}; ^{1}H NMR (300 MHz, DMSO-d_6): $\delta = 5.23$ (s, 1H), 7.1–7.3 (m, 6H), 7.6–7.7 (m, 2H), 8.3–8.4 (m, 1H), 8.9–9.0 (m, 1H); ^{13}C NMR (75.5 MHz, DMSO-d_6): $\delta = 36.0$, 53.7, 115.5–116.6 (m), 117.3–117.8 (m), 119.8, 120.0, 122.3, 123.8, 126.3, 127.9, 133.5–133.8 (m), 136.0, 137.4, 143.4, 150.3, 154.8–159.8 (m), 160.7; EIMS *m/z* 335 (83) [M$^+$], 291 (12), 222 (100), 195 (18); Anal. Calcd. for $C_{19}H_{11}F_2N_3O$: C, 68.06; H, 3.31; N, 12.53. Found: C, 68.10; H, 3.33; N, 12.50.

2-Amino-4-(3-fluoro-4-methoxyphenyl)-4*H*-pyrano[3,2-*h*]quinolone-3-carbonitrile (2i)

After the reaction, water was added and the aqueous phase was extracted with ethyl acetate. The organic phase was dried over Na_2SO_4, filtered and the filtrate was concentrated. The obtained residue was recrystallized from CH_2Cl_2/*n*-hexane. Off-white solid; yield: 34%; mp 99–102 °C; IR (ATR) υ_{max} 3340, 3182, 2937, 2843, 2190, 1654, 1599, 1569, 1515, 1465, 1443, 1405, 1389, 1371, 1317, 1271, 1222, 1185, 1109, 1056, 1022, 939, 837, 778, 761, 749, 667, 644 cm^{-1}; ^{1}H NMR (300 MHz, DMSO-d_6):

δ = 3.80 (s, 3H), 4.95 (s, 1H), 7.0–7.3 (m, 6H), 8.3–8.4 (m, 1H), 8.9–9.0 (m, 1H); ^{13}C NMR (75.5 MHz, DMSO-d_6): δ = 43.8, 56.0, 114.1, 115.4, 121.6, 122.2, 123.6, 123.8, 126.8, 127.7, 136.0, 138.6, 142.9, 150.2, 160.2; EIMS *m/z* 347 (26) [M^+], 312 (10), 248 (12), 222 (67), 202 (100), 187 (38), 159 (23), 145 (22), 139 (27), 132 (35), 117 (11), 84 (22), 57 (16); Anal. Calcd. for $C_{20}H_{14}FN_3O_2$: C, 69.16; H, 4.06; N, 12.10. Found: C, 69.07; H, 4.00; N, 12.03.

2-Amino-4-(3,5-difluorophenyl)-9-methyl-4*H*-pyrano[3,2-*h*] quinolone-3-carbonitrile (3a)

Colorless solid; yield 30%; mp 275–277 °C; IR (ATR) υ_{max} 3469, 3352, 3102, 3054, 2186, 1651, 1620, 1578, 1558, 1505, 1452, 1441, 1401, 1388, 1378, 1319, 1311, 1273, 1238, 1222, 1196, 1184, 1146, 1119, 1107, 1012, 995, 985, 893, 868, 860, 845, 828, 814, 795, 748, 728, 693, 683 cm^{-1}; ^{1}H NMR (300 MHz, $CDCl_3$/DMSO-d_6): $\delta = 2.69$ (s, 3H), 4.78 (s, 1H), 6.6–6.8 (m, 5H), 7.03 (d, $J = 8.5$ Hz, 1H), 7.33 (d, $J = 8.4$ Hz, 1H), 7.45 (d, $J = 8.5$ Hz, 1H), 8.01 (d, $J =$ 8.4 Hz, 1H); ^{13}C NMR (75.5 MHz, $CDCl_3$/DMSO-d_6): $\delta =$ 24.1, 40.2, 55.1, 100.8–101.5 (m), 109.3–109.7 (m), 118.8, 119.0, 121.6, 122.3, 124.2, 125.2, 134.7, 136.2, 141.8, 148.2, 157.9, 159.3, 159.8–160.0 (m), 163.1–163.3 (m); EIMS *m/z* 349 (93) $[M]^+$, 305 (13), 237 (56), 236 (100), 209 (20); Anal. Calcd. for $C_{20}H_{13}F_2N_3O$: C, 68.76; H, 3.75; N, 12.03. Found: C, 68.69; H, 3.70; N, 11.99.

2-Amino-4-(3-fluorophenyl)-9-methyl-4*H*-pyrano[3,2-*h*] quinolone-3-carbonitrile (3b)

Colorless solid; yield 30%; mp 307–308 °C; IR (ATR) υ_{max} 3465, 3347, 2188, 1655, 1625, 1614, 1580, 1506, 1483, 1453, 1440, 1401, 1379, 1317, 1272, 1260, 1239, 1221, 1192, 1134, 1108, 1010, 947, 901, 847, 786, 766, 755, 718, 694, 668 cm^{-1}; ^{1}H NMR (300 MHz, $CDCl_3$/DMSO-d_6): $\delta = 2.58$ (s, 3H), 4.69 (s, 1H), 5.63 (s, 2H), 6.7–6.8 (m, 2H), 6.8–6.9 (m, 2H), 7.0–7.1 (m, 1H), 7.17 (d, $J = 8.4$ Hz, 1H), 7.2–7.3 (m, 1H), 7.82 (d, $J = 8.4$ Hz, 1H); ^{13}C NMR (75.5 MHz, $CDCl_3$/DMSO-d_6): $\delta = 25.1$, 41.2, 58.0, 113.7–114.6 (m), 119.6, 120.5, 122.5, 123.2, 125.4, 126.1, 129.8–129.9 (m), 135.6, 137.2, 142.6, 147.0, 159.1, 159.7, 160.9, 164.2; ESIMS *m/z* 332.1 (100) $[M]^+$, 266.0 (90); Anal. Calcd. for $C_{20}H_{14}FN_3O$: C, 72.50; H, 4.26; N, 12.68. Found: C, 72.60; H, 4.30; N, 12.72.

2-Amino-4-(3-nitrophenyl)-9-methyl-4*H*-pyrano[3,2-*h*] quinolone-3-carbonitrile (3d)

Amber solid; yield 31%; mp 248–249 °C; IR (ATR) υ_{max} 3332, 3199, 2191, 1666, 1628, 1599, 1522, 1476, 1440, 1406, 1347, 1319, 1303, 1276, 1240, 1222, 1195, 1143, 1114, 1098, 1082, 1059, 1023, 919, 907, 842, 817, 804, 786, 749, 739, 716, 680 cm^{-1}; ^{1}H NMR (300 MHz, $CDCl_3$): $\delta = 2.78$ (s, 3H), 5.02 (s, 1H), 5.42 (s, 2H), 7.00 (d, $J = 8.5$ Hz, 1H), 7.37 (d, $J = 8.4$ Hz, 1H), 7.4–7.5 (m, 2H), 7.6–7.7 (m, 1H), 8.01 (d, $J = 8.4$ Hz, 1H), 8.0–8.1 (m, 2H); ^{13}C NMR (75.5 MHz, $CDCl_3$): $\delta = 25.3$, 41.6, 58.8, 119.4, 120.2, 122.7, 122.9, 123.4, 124.0, 125.6, 126.8, 130.0, 134.1, 136.3, 137.5, 143.0, 146.5, 148.8, 160.0; EIMS *m/z* 358 (97) $[M]^+$, 237 (95), 236 (100), 209 (33); Anal. Calcd. for $C_{20}H_{14}N_4O_3$: C, 67.03; H, 3.94; N, 15.63. Found: C, 66.99; H, 3.91; N, 15.60.

2-Amino-4-(2-fluorophenyl)-9-methyl-4*H*-pyrano[3,2-*h*] quinolone-3-carbonitrile (3e)

Off-white solid; yield 35%; mp 302 °C; IR (ATR) υ_{max} 3324, 3192, 2196, 1660, 1631, 1602, 1508, 1488, 1453, 1505, 1322, 1281, 1239, 1197, 1113, 1094, 1030, 844, 819, 808, 758, 747, 707, 670, 616 cm^{-1}; ^{1}H NMR (300 MHz, $CDCl_3$/DMSO-d_6): $\delta = 2.70$ (s, 3H), 5.19 (s, 1H), 5.93 (s, 2H), 6.9–7.0 (m, 5H), 7.27 (d, $J = 8.5$ Hz, 1H), 7.37 (d, $J =$ 8.5 Hz, 1H), 7.94 (d, $J = 8.4$ Hz, 1H); ^{13}C NMR (75.5 MHz, $CDCl_3$): $\delta = 24.8$, 34.4, 56.3, 114.8–115.2 (m), 119.5, 120.3, 122.2, 123.0, 124.1, 124.9, 125.8, 128.3–128.4 (m), 129.5, 130.8–131.0 (m), 135.4, 136.9, 142.6, 157.8, 158.7, 160.2, 161.1; EIMS *m/z* 331 (37) $[M]^+$, 236 (100); Anal. Calcd. for $C_{20}H_{14}FN_3O$: C, 72.50; H, 4.26; N, 12.68. Found: C, 72.44; H, 4.30; N, 12.65.

2-Amino-4-(3-bromophenyl)-9-methyl-4*H*-pyrano[3,2-*h*] quinolone-3-carbonitrile (3f)

Off-white solid; yield 62%; mp 157–158 °C; IR (ATR) υ_{max} 3325, 3181, 2202, 2180, 1656, 1628, 1604, 1570, 1509, 1474, 1444, 1424, 1403, 1323, 1282, 1237, 1182, 1144, 1107, 1072, 1046, 1023, 997, 866, 842, 831, 792, 775, 747, 721, 694, 678, 621 cm^{-1}; ^{1}H NMR (300 MHz, $CDCl_3$): $\delta =$ 2.78 (s, 3H), 4.83 (s, 1H), 5.21 (s, 2H), 7.02 (d, $J = 8.5$ Hz, 1H), 7.1–7.3 (m, 5H), 7.43 (d, $J = 8.5$ Hz, 1H), 8.00 (d, $J =$ 8.4 Hz, 1H); ^{13}C NMR (75.5 MHz, $CDCl_3$): $\delta = 25.4$, 41.5, 59.5, 119.6, 121.0, 122.7, 123.1, 123.8, 125.9, 126.6, 126.7, 130.4, 130.7, 131.1, 136.3, 137.5, 142.9, 146.6, 159.8; EIMS *m/z* 393 (66) $[M]^+$, 391 (66) $[M]^+$, 328 (18), 326 (19), 237 (100), 236 (99), 209 (32); Anal. Calcd. for $C_{20}H_{14}BrN_3O$: C, 61.24; H, 3.60; N, 10.71. Found: C, 61.27; H, 3.58; N, 10.74.

2-Amino-4-(2,3-difluorophenyl)-9-methyl-4*H*-pyrano[3,2-*h*] quinolone-3-carbonitrile (3g)

Colorless solid; yield: 32%; mp 250–252 °C; IR (ATR) υ_{max} 3461, 3344, 2189, 1652, 1623, 1606, 1581, 1508, 1485, 1443, 1403, 1390, 1379, 1318, 1267, 1239, 1224, 1200, 1145, 1109, 1065, 1014, 971, 958, 844, 828, 814, 801, 791,

779, 756, 736, 721, 697, 657, 603 cm^{-1}; ^1H NMR (300 MHz, DMSO-d_6): δ = 2.70 (s, 3H), 5.28 (s, 1H), 7.0–7.3 (m, 6H), 7.49 (d, J = 8.5 Hz, 1H), 7.61 (d, J = 8.5 Hz, 1H), 8.22 (d, J = 8.5 Hz, 1H); ^{13}C NMR (75.5 MHz, DMSO-d_6): δ = 25.0, 35.6, 54.1, 116.2–116.4 (m), 119.9–120.0 (m), 123.0, 123.7, 125.0–125.3 (m), 126.3, 134.5–134.6 (m), 136.1, 136.9, 143.0, 146.1–146.3 (m), 148.1–148.3 (m), 149.5–149.5 (m), 151.4–151.5 (m), 159.2, 160.7; EIMS *m/z* 349 (54) [M^+], 305 (7), 236 (100), 209 (12), 175 (6); Anal. Calcd. for $C_{20}H_{13}F_2N_3O$: C, 68.76; H, 3.75; N, 12.03. Found: C, 68.73; H, 3.72; N, 12.07.

2-Amino-4-(2,5-difluorophenyl)-9-methyl-4*H*-pyrano[3,2-*h*] quinolone-3-carbonitrile (3h)

Off-white solid; yield: 49%; mp 257–259 °C; IR (ATR) υ_{max} 3357, 3184, 3075, 2977, 2197, 1655, 1632, 1603, 1510, 1488, 1444, 1427, 1403, 1321, 1283, 1256, 1239, 1171, 1141, 1113, 1087, 1043, 956, 889, 870, 839, 830, 813, 788, 747, 721, 696, 670, 659, 638, 619 cm^{-1}; ^1H NMR (300 MHz, DMSO-d_6): δ = 2.70 (s, 3H), 5.20 (s, 1H), 7.1–7.3 (m, 6H), 7.49 (d, J = 8.4 Hz, 1H), 7.61 (d, J = 8.4 Hz, 1H), 8.22 (d, J = 8.4 Hz, 1H); ^{13}C NMR (75.5 MHz, DMSO-d_6): δ = 25.0, 36.1, 53.9, 115.5–116.6 (m), 117.3–117.6 (m), 119.8, 120.1, 123.0, 123.6, 125.3, 126.3, 133.8, 136.1, 136.9, 143.0, 154.7–159.8 (m), 159.1, 160.7; EIMS *m/z* 347 (26) [M^+], 312 (10), 248 (12), 222 (67), 202 (100), 187 (38), 159 (23), 145 (22), 139 (27), 132 (35), 117 (11), 84 (22), 57 (16); Anal. Calcd. for $C_{20}H_{13}F_2N_3O$: C, 68.76; H, 3.75; N, 12.03. Found: C, 68.80; H, 3.79; N, 12.08.

2-Amino-4-(3-fluoro-4-methoxyphenyl)-9-methyl-4*H*-pyrano[3,2-*h*]quinolone-3-carbonitrile (3i)

After the reaction, water was added and the aqueous phase was extracted with ethyl acetate. The organic phase was dried over Na_2SO_4, filtered and the filtrate was concentrated. The obtained residue was recrystallized from CH_2Cl_2/*n*-hexane. Off-white solid; yield: 33%; mp 109–111 °C; IR (ATR) υ_{max} 3341, 3193, 2964, 2939, 2843, 2191, 1653, 1621, 1603, 1514, 1464, 1442, 1400, 1322, 1272, 1224, 1184, 1119, 1023, 943, 875, 845, 798, 762, 749, 721 cm^{-1}; ^1H NMR (300 MHz, DMSO-d_6): δ 2.70 (s, 3H), 3.80 (s, 3H), 4.92 (s, 1H), 7.0–7.2 (m, 6H), 7.4–7.5 (m, 1H), 7.5–7.6 (m, 1H), 8.2–8.3 (m, 1H); ^{13}C NMR (75.5 MHz, DMSO-d_6): δ = 25.0, 43.8, 56.0, 114.1, 114.9, 115.1, 121.6, 122.8, 123.4, 123.8, 125.8, 126.1, 127.5, 136.1, 137.0, 138.7, 142.5, 153.0, 159.0, 160.3; EIMS *m/z* 361 (38) [M^+], 296 (11), 236 (100), 159 (23), 140 (14), 91 (30); Anal. Calcd. for $C_{21}H_{16}FN_3O_2$: C, 69.80; H, 4.46; N, 11.63. Found: C, 69.74; H, 4.42; N, 11.58.

Cell culture conditions

518A2 (Department of Radiotherapy, Medical University of Vienna, Austria) melanoma, Panc-1 (ACC-783) pancreatic ductular adenocarcinoma, KB-V1^{Vbl} (ACC-149) cervix carcinoma, MCF-7^{Topo} (ACC-115) breast carcinoma, HT-29 (ACC-299), HCT-116 (ACC-581), DLD-1 (ACC-278) colon carcinoma cells were cultivated in Dulbecco's Modified Eagle Medium (DMEM) supplemented with 10% fetal bovine serum, and 1% antibiotic-antimycotic at 37 °C, 5% CO_2, and 95% humidity. To keep MCF-7^{Topo} and KB-V1^{Vbl} cells resistant, the maximum-tolerated dose of topotecan or vinblastine, respectively, were added to the cell culture medium 24 h after every passage. Human dermal fibroblasts HDFa (ATCC: PCS-201-202^{TM}) were cultivated in DMEM with FBS (10%), Antibiotic-Antimycotic (1%) and glutamine (2 mM) at 37 °C in humidified atmosphere (95% humidity) with 5% CO_2. Mycoplasma-free cell cultures were used only.

MTT assay

The assay was performed following a literature procedure (Mosmann 1983). Cells (cancer cells: 5×10^4 cells/mL, 100 µL/well; HDFa: 1×10^5 cells/mL, 100 µL/well) were grown in 96-well plates for 24 h. Then, they were treated with the test compounds (various concentrations) or with vehicle (DMSO) only for 72 h at 37 °C. MTT solution (12.5 µL of a 0.5% MTT solution in PBS) was added to the cells whereupon they were incubated for 2 h at 37 °C. The plates were centrifuged (300 × *g*, 5 min, 4 °C), the medium was withdrawn, and the formed formazan was dissolved in 25 µL of DMSO containing 10% SDS and 0.6% acetic acid for at least 2 h at 37 °C. Formazan absorbance (λ = 570 nm) and background (λ = 630 nm) were measured with a microplate reader (Tecan). IC_{50} values were calculated from the dose-inhibition curves as the means ± SD of four independent experiments with respect to vehicle-treated control cells set to 100%.

DFCH-DA assay

518A2 melanoma cells (1×10^5 cells/mL, 50 µL/well) were incubated in a black 96-well plate for 24 h. The medium was exchanged for serum-free DMEM supplemented with 20 µM DCFH-DA (2′,7′-dichlorohydrofluorescein diacetate, Sigma Aldrich) and incubated for 30 min at 37 °C. The cells were washed twice with 100 µL PBS and 100 µL of serum-free DMEM was added. Then, the cells were treated with **3a** and **3d** (0, 1, 5, and 10 µM) for 1 h at 37 °C. The cells were washed twice with 100 µL PBS and the plate was immediately placed in a microplate reader (TECAN). DCF fluorescence (λ_{ex} = 485 nm; λ_{em} = 535 nm) as a measure of

intracellular ROS levels was determined and the fluorescence of untreated control cells was set to 100%. Values exceeding 100% indicate increased ROS concentrations in the cells. ROS generation (%) was depicted as the mean ± SD of five independent experiments.

Tubulin polymerization assay

Brinkley's buffer 80 (BRB80, 50 µL) supplemented with 20% glycerol and GTP (3 mM) were added to a black 96-well half-area plate with clear bottom. The test compounds, CA-4, **3a** and **3d** at final concentrations of 2.5 µM, 5 µM, 10 µM, or vehicle (DMSO) were added. Then, 50 µL tubulin in BRB80 (10 mg/mL) was added to the wells and the plate was immediately placed in a pre-heated microplate reader (Tecan). The polymerization was determined at 37 °C by measurement of the absorption at 340 nm for 120 min in intervals of 5 min.

Immunofluorescence staining of microtubule cytoskeleton

518A2 melanoma cells (5×10^4 cells/mL, 500 µL/well) were given in 24-well plates on glass coverslips and cultivated for 24 h. Then, **3d** (100, 250, and 500 nM) or vehicle (DMSO) were added to the cells and the cells were incubated for 24 h. After a washing step with PBS, the cells were fixed in 3.7% formaldehyde in PBS (20 min, rt), permeabilized and blocked in 1% BSA and 0.1% triton X-100 in PBS (30 min, rt). Incubation of the cells with monoclonal mouse anti-alpha-tubulin antibody (1 h, 37 °C) followed. Then, the cells were washed for three times with PBS and treated with the secondary anti-mouse 488 antibody conjugate (1 h, rt, in the dark). The cells were washed again for three times with PBS and once with water. Then, mounting the glass coverslips with 4–88 based mounting medium supplemented with 2.5% DABCO and 1 µg/mL DAPI for counterstaining the nuclei was carried out. Images of the microtubules were documented by a Zeiss Imager A1 AX10 fluorescence microscope (×400 magnification).

Chorioallantoic membrane (CAM) assay in fertilized chicken eggs

The experiment was carried out according to a literature procedure (Nitzsche et al. 2010). Incubation of fertilized white leghorn chicken eggs (SPF eggs, VALO Biomedia) at 37 °C and 50–60% humidity until day 5 past fertilization was followed by cutting windows of 2–3 cm diameter in the more rounded pole of the eggshell which were sealed with tape. The eggs were incubated for 24 h and silicon foil rings (5 mm diameter) were placed onto the CAM whereupon 5 nmol of **3a**, 10 nmol of **3d** or vehicle (DMSO) were pipetted inside the rings. Changes in the organization of the blood vessel were documented after 0, 6, and 24 h post application using a light microscope (60-fold magnification, Traveller). The CAMs of at least three eggs treated with test compounds were analyzed.

Acknowledgements We thank Madeleine Gold and Kerstin Hannemann (Organic Chemistry 1, University of Bayreuth) for technical assistance.

Compliance with ethical standards

Conflict of interest The authors declare that they have no conflict of interest.

References

Afzal O, Kumar S, Haider MR, Ali MR, Kumar R, Jaggi M, Bawa S (2015) A review on anticancer potential of bioactive heterocycle quinoline. Eur J Med Chem 97:871–910

Birch KA, Heath WF, Hermeling RN, Johnston CM, Stramm L, Dell C, Smith C, Williamson JR, Reifel-Miller A (1996) LY290181, an inhibitor of diabetes-induced vascular dysfunction, blocks protein kinase C-stimulated transcriptional activation through inhibition of transcription factor binding to a phorbol response element. Diabetes 45:642–650

Dgachi Y, Sokolov O, Luzet V, Godyn J, Panek D, Bonet A, Martin H, Iriepa I, Moraleda I, García-Iriepa C, Janockova J, Richert L, Soukup O, Malawska B, Chabchoub F, Marco-Contelles J, Ismaili L (2017) Tetrahydropyranodiquinolin-8-amines as new, non hepatoxic, antioxidant, and acetylcholinesterase inhibitors for Alzheimer's disease therapy. Eur J Med Chem 126:576–589

El-Agrody AM, Al-Ghamdi AM (2011) Synthesis, of novel 4*H*-pyrano[3,2-*h*]quinoline derivatives. ARKIVOC 11:134–146

El-Agrody AM, Abd-Rabboh HSM, Al-Ghamdi AM (2013) Synthesis, antitumor activity, and structure-activity relationship of some 4*H*-pyrano[3,2-*h*]quinoline and 7*H*-pyrimidino[4',5':6,5]pyrano[3,2-*h*]quinoline derivatives. Med Chem Res 22:1339–1355

Fouda AM (2017) Halogenated 2-amino-4H-pyrano[3,2-h]quinolone-3-carbonitriles as antitumor agents and structure-activity relationships of the 4-, 6-, and 9-positions. Med Chem Res 26:302–313

Gold M, Mujahid Y, Ahmed K, Kostrhunova H, Kasparkova J, Brabec V, Biersack B, Schobert R (2019) A new 4-(pyridinyl-4*H*-benzo[*g*]chromene-5,10-dione ruthenium(II) complex inducing senescence in 518A2 melanoma cells. J Biol Inorg Chem. https://doi.org/10.1007/s00775-019-01677-y

Isanbor C, O'Hagan D (2006) Fluorine in medicinal chemistry: A review of anticancer agents. J Fluor Chem 127:303–319

Kemnitzer W, Drewe J, Jiang S, Zhang H, Zhao J, Crogan-Grundy C, Xu L, Lamothe S, Gourdeau H, Denis R, Tseng B, Kasibhatla S, Cai SX (2007) Discovery of 4-aryl-4*H*-chromenes as a new series of apoptosis inducers using a cell- and caspase-based high-throughput screening assay. 3. Structure – activity relationships of fused rings at the 7,8-positions. J Med Chem 50:2858–2864

Kumar S, Bawa S, Gupta H (2009) Biological activities of quinoline derivatives. Mini-Rev Med Chem 9:1648–1654

Lau ATY, Wang Y, Chiu JF (2008) Reactive oxygen species: current knowledge and applications in cancer research. J Cell Biochem 104:657–667

Lippert III JW (2007) Vascular disrupting agents. Bioorg Med Chem 15:605–615

Mahal K, Biersack B, Schobert R (2013) New oxazole-bridged combretastatin A-4 analogues as potential vascular-disrupting agents. Int J Clin Pharm Ther 51:41–43

Mosmann T (1983) Rapid colorimetric assay for cellular growth and survival: application to proliferation and cytotoxicity assays. J Immunol Methods 65:55–63

Nitzsche B, Gloesenkamp C, Schrader M, Ocker M, Preissner R, Lein M, Zakrzewicz A, Hoffmann B, Höpfner M (2010) Novel compounds with antiangiogenic and antiproliferative potency for growth control of testicular germ cell tumours. Br J Cancer 103:18–28

Pérez-Pérez M-J, Priego E-M, Bueno O, Martins MS, Canela M-D, Liekens S (2016) Blocking blood flow to solid tumors by destabilizing tubulin: an approach to targeting tumor growth. J Med Chem 59:8685–8711

Rafinejad A, Fallah-Tafti A, Tiwari R, Shirazi AN, Mandal D, Shafiee A, Parang K, Foroumadi A, Akbarzadeh T (2012) 4-Aryl-4*H*-naphthopyrans derivatives: one-pot synthesis, evaluation of Src kinase inhibitory and anti-proliferative activities. DARU J Pharm Sci 20:100

Schmitt F, Kasparkova J, Brabec V, Begemann G, Schobert R, Biersack B (2018) New (arene)ruthenium(II) complexes of 4-aryl-4*H*-naphthopyrans with anticancer and anti-vascular activities. J Inorg Biochem 184:69–78

Schmitt F, Gold M, Rothemund M, Andronache I, Biersack B, Schobert R, Mueller T (2019) New naphthopyran analogues of LY290181 as potential tumor vascular-disrupting agents. Eur J Med Chem 163:160–168

Smith W, Bailey JM, Billingham MEJ, Chandrasekhar S, Dell CP, Harvey AK, Hicks CA, Kingston AE, Wishart GN (1995) The anti-rheumatic potential of a series of 2,4-di-substituted-4H-naphthol[1,2-b]pyran-3-carbonitriles. Bioorg Med Chem Lett 5:2783–2788

Thorpe PE (2002) Vascular targeting agents as cancer therapeutics. Clin Cancer Res 10:415–427

Thumar NJ, Patel MP (2009) Synthesis and in vitro antimicrobial evaluation of 4H-pyrazolopyran, -benzopyran and naphthopyran derivatives of 1H-pyrazole. Arkivoc 13:363–380

Tron GC, Pirali T, Sorba G, Pagliai F, Busacca S, Genazzani AA (2006) Medicinal chemistry of combretastatin A4: present and future directions. J Med Chem 49:3033–3044

Upadhyay KD, Dodia NM, Khunt RC, Chaniara RS, Shah AK (2018) Synthesis and biological screening of pyrano[3,2-c]quinolone analogues as anti-inflammatory and anticancer agents. ACS Med Chem Lett 9:283–288

Wiernicki TR, Bean JS, Dell C, Williams A, Wood D, Kauffman RF, Singh JP (1996) Inhibition of vascular smooth muscle cell proliferation and arterial intimal thickening by a novel antiproliferative naphthopyran. J Pharm Exp Ther 278:1452–1459

Wood D, Panda D, Wiernicki TR, Wilson L, Jordan MA, Singh JP (1997) Inhibition of mitosis and microtubule function through direct tubulin binding by a novel antiproliferative naphthopyran LY290181. Mol Pharm 52:427–444